Fish and Shellfish Immunology 89 (2019) 632–640

Contents lists available at ScienceDirect

Fish and Shellfish Immunology

journal homepage: www.elsevier.com/locate/fsi

Full length article

# Iron regulatory protein is involved in the immune defense of the Chinese mitten crab *Eriocheir sinensis*

Lei Yang, Xuejie Li, Yaomeng Wu, Jiashun Zhang, Weiwei Li, Qun Wang*

*Laboratory of Invertebrate Immunological Defense and Reproductive Biology, School of Life Sciences, East China Normal University, Shanghai, China*

ARTICLE INFO

*Keywords:*
*Eriocheir sinensis*
Iron regulatory protein
Iron-responsive element
Bacterial challenge

ABSTRACT

Iron homeostasis is vital to organismal health; it is maintained by the iron regulatory protein (IRP)–iron-responsive element (IRE) signaling pathway. In the Chinese mitten crab *Eriocheir sinensis*, *Es*Fer-1 and *Es*Fer-2 reportedly have a putative IRE, but an IRP has not yet been identified. In this study, we successfully amplified the full-length cDNA of *Es*IRP using gene cloning and rapid amplification of cDNA ends techniques. The length of this cDNA was 4474 bp, and it included a 2682-bp open reading frame encoding 893 amino acids. Using quantitative real-time PCR, mRNA transcripts of *Es*IRP were detected in various tissues. The highest and lowest expression level was detected in the muscle and gills, respectively. In response to *Staphylococcus aureus* and *Vibrio parahaemolyticus* challenge, the transcription level of *Es*IRP was downregulated and that of *Es*Fer-1 and *Es*Fer-2 was upregulated in hemocytes. *Es*IRP knockdown resulted in increased expression of both *Es*Fer-1 and *Es*Fer-2. After *Es*Fer-1 and *Es*Fer-2 knockdown, the bacterial clearance ability of *E. sinensis* against *S. aureus* and *V. parahaemolyticus* was impaired. In conclusion, our results suggest that the IRP–IRE signaling pathway plays an important role in the innate immune system response in *E. sinensis*.

## 1. Introduction

The innate immune system acts as the frontline of defense against microbial pathogens by recognizing pathogen-associated molecular patterns using pattern recognition receptors [1]. With the accumulation of knowledge about how hosts fight infections, immunologists have realized that pathogen recognition is only one of the facets of innate immunity. The iron-withholding strategy in innate immunity has gradually caught the attention of many researchers [2]. Iron plays a key role in infectious diseases; it can be used not only as a regulator of the innate immune system response but also as a nutrient source for microorganisms [3,4]. Although a sufficient amount of electron transfer is required in alkaline biochemical reactions, excess iron may be harmful because it can catalyze the non-enzymatic production of toxic oxygen intermediates via Fenton/Haber–Weiss chemistry [5]. Iron is involved in diverse metabolic and synthetic pathways that unicellular and multicellular organisms rely on; microbes including bacterial, protozoan and fungal pathogens also have an essential requirement of iron [6–8]. Therefore, all organisms have evolved complex mechanisms to maintain cellular iron homeostasis. The hormone hepcidin, produced by the liver, is believed to be the central regulator of systemic iron homeostasis [9]. Other than this, there is a distinct iron regulatory system that maintains iron homeostasis by regulating the levels of transferrin receptors and other proteins in individual cells [10].

Iron homeostasis is meticulously regulated by the iron regulatory protein (IRP)–iron-responsive element (IRE) signaling pathway at the transcription level [11]. IRP can control the translation of ferritin and ferroportin mRNA as well as the stability of transferrin receptor mRNA by interacting with their IRE function [12]. Ferritin both in the cytoplasm and mitochondria can sequester and store iron in the ferric state [13,14]. Excess iron is mainly exported to blood through ferroportin [15]. Transferrin then binds iron in the ferric state and transports it to the peripheral tissues. The iron-loaded transferrin binds to the cell surface transferrin receptor and undergoes endocytosis [11]. IRE is a specific non-coding sequence located on the untranslated region (UTR) of mRNA transcripts and contains the classic CAGUGN sequence [12]. IRE motifs are located in the 5′-UTR of ferritin H and L subunits, ferroportin, and aminolevulinic acid synthetase and in the 3′-UTR of transferrin receptor and divalent metal transporter 1 (DMT1) [11]. When iron is deficient in cells, IRPs can bind to IRE motifs in the 5′-UTR to abrogate target mRNA translation. However, when iron is in excess, it can bind to IRP and dissociate IRP from target genes, inducing normal translation [12]. In contrast, IRP binding to IRE motifs in the 3′-UTR can promote translation of target mRNA against endonuclease cleavage [12]. When IRP dissociates from IRE motifs in the 3′-UTR, the target mRNA becomes susceptible to endonuclease attack and degradation.

* Corresponding author.
*E-mail address:* qwang@bio.ecnu.edu.cn (Q. Wang).

https://doi.org/10.1016/j.fsi.2019.04.041
Received 25 December 2018; Received in revised form 4 April 2019; Accepted 11 April 2019
Available online 14 April 2019

Under conditions of iron deficiency, as ferritin and ferroportin mRNAs have IREs in their 5′-UTRs, their translation is inhibited by IRPs; however, as transferrin receptor and DMT1 mRNAs have IREs in their 3′-UTRs, their translation is promoted by IRPs [11]. In contrast, when iron is in excess, IRP dissociation from IREs promotes the translation of ferritin and ferroportin mRNAs but destabilizes transferrin receptor and DMT1 mRNAs [12]. The importance of IRPs for innate immunity was discovered by the genetic disruption of the macrophage IRP-IRE system in mice [16,17]. IRP ablation in macrophages broadly hampers the immune response to *Salmonella* infection [18]. It also seems to promote toll-like receptor signaling [19].

The Chinese mitten crab *Eriocheir sinensis* is an important commercial aquaculture species in China and other Asian countries. The continuous expansion of aquaculture has given rise to many problems; diseases caused by bacteria, viruses, and parasites are known to cause serious economic losses [20–22]. Therefore, it is necessary to study the immune mechanism of *E. sinensis*. In recent years, some iron-binding proteins have been reported in *E. sinensis*. Two novel ferritins containing IREs in the 5′-UTR have been identified from Chinese mitten crabs. In response to *Listonella anguillarum* and *Pichia pastoris GS115* challenge, the expression levels of both *Es*Fer-1 and *Es*Fer-2 are upregulated in hemocytes [23]. Transferrin and ferritin reportedly participate in the immune response to *Spiroplasma eriocheiris* in *E. sinensis* [24]. In this study, we identified an IRP, *Es*IRP, and analyzed its tissue expression profiles. *Es*IRP expression levels were investigated after bacterial challenge. RNA interference (RNAi) of *Es*Fer-1 and *Es*Fer-2 impaired bacterial clearance. Our results suggest that the IRP–IRE signaling pathway plays an important role in the innate immune system response in *E. sinensis*.

## 2. Material and methods

### 2.1. Animals

Healthy adult male Chinese mitten crabs (n = 240; wet weight = 100 ± 15 g) were purchased from a local agricultural market in Shanghai, China. They were acclimated for 1 week at 23 °C ± 2 °C in aerated freshwater with abundance of oxygen before being used for experiments. Before use, 5% of crabs was randomly detected by PCR using TaKaRa 16S rDNA Bacterial Identification PCR Kit to ensure that the crab were free of *Staphylococcus aureus* and *Vibrio parahemolyticus*.

### 2.2. Bacterial challenge and sample collection

The Gram-positive bacterium *Staphylococcus aureus* and the Gram-negative bacterium *Vibrio parahaemolyticus* were gifted by the National Pathogen Collection Center for Aquatic Animals (Shanghai Ocean University, Shanghai, China). Bacteria were cultured overnight in Luria–Bertani (LB) medium at 37 °C and collected by centrifugation at 5000 × *g* for 5 min, washed three times, and then resuspended in sterile PBS (137 mM NaCl, 2.7 mM KCl, 10 mM $Na_2HPO_4$, 2 mM $KH_2PO_4$, pH 7.4). Numbers of bacterial colony-forming units (CFU) were determined by plating the diluted suspension onto agar plates. For the bacterial challenge experiment, the crabs were randomly divided into three groups. In the two challenge groups, the animals were separately injected with 200 μl *S. aureus* or *V. parahaemolyticus* ($1 \times 10^8$ CFU) using a microliter syringe. In the control group, the crabs were injected with the same volume of PBS. At specific time points (0 h, 6 h, 12 h, 24 h, and 48 h) after bacterial challenge, hemolymph samples were collected from the ventral sinus via the arthrodial membrane at the base of a walking leg using a sterile syringe containing an equal volume of an anticoagulant solution (0.1 M glucose, 30 mM citrate, 26 mM citric acid, 0.14 M NaCl, and 10 mM ethylenediaminetetraacetic acid). The solution was then transferred to a centrifuge tube and immediately centrifuged at 800 × *g* for 15 min at 4 °C to obtain hemocytes. Subsequently, other tissues including the hepatopancreas, stomach, gills, muscle, intestine, and heart were collected. The samples were immediately frozen in liquid nitrogen and stored at −80 °C. Three crabs were chosen for each sample in case of individual differences.

### 2.3. Total RNA extraction and cDNA synthesis

Total RNA was extracted from the aforementioned tissues using Trizol (RNA extraction kit, Invitrogen), according to manufacturer's instructions. The integrity of extracted RNA samples was detected using agarose gel electrophoresis, and the samples were quantified by UV spectrophotometry. RNA concentration and purity were checked using a NanoDrop 2000 spectrophotometer (Thermo Fisher Scientific, Wilmington, DE). The cDNA template for general PCR was synthesized using the PrimeScript™ First-Strand cDNA Synthesis Kit (Takara, Shiga, Japan), according to manufacturer's instructions. Total RNA was reverse transcribed using the SMARTer® RACE cDNA Amplification Kit (Clontech, Shiga, Japan) for rapid amplification of cDNA ends (RACE) and PrimeScript™ RT reagent Kit with gDNA Eraser (Takara) for quantitative real-time PCR (qRT-PCR).

### 2.4. Gene cloning of EsIRP

The *Es*IRP partial cDNA sequence was obtained from the transcriptome data of *E. sinensis*. The partial cDNA was amplified using general PCR. The complete sequence of the *Es*IRP gene was extended using 3′- and 5′-RACE. Gene-specific primers (Table 1) were designed based on the partial cDNA sequences, and amplification was performed according to the instructions of different kits. PCR products were purified and inserted into the pEASY-T1 vector (TransGen, China) for DNA sequencing.

### 2.5. Sequence analysis

The open reading frame (ORF) of *Es*IRP was identified using ORF finder (http://www.ncbi.nlm.nih.gov/gorf/orfig.cgi). Full-length cDNA and the deduced amino acid sequences were compared against sequences from other representative vertebrates and invertebrates deposited in the National Center for Biotechnology Information (NCBI) GenBank using BLAST (https://blast.ncbi.nlm.nih.gov/Blast.cgi). Molecular weight and estimated isoelectric point (pI) of the *Es*IRP protein were predicted using the ProtParam tool of ExPASy (https://

**Table 1**
Primer sequences.

| Primer name and purpose | Sequence (5′–3′) |
|---|---|
| **cDNA cloning** | |
| RT-IRP-F | GTACCATCGTTGTCAGGTCC |
| RT-IRP-R | GCTGAACACTATCCGCAGAA |
| 5RACE-IRP-1 | GGATGTGGAGGGTGCGCGGT |
| 5RACE-IRP-2 | CGCGGTCCAGCCTTCTTGGCA |
| 5RACE-IRP-3 | AGCCCGGCGAGAGGGAGGTC |
| 3RACE-IRP-1 | ACAGGGTGCCGGTGTCTGGGA |
| 3RACE-IRP-2 | TGGCTCGGTGGTCATTGCGGC |
| 3RACE-IRP-3 | GGCTGGCTCCATCGCACGCA |
| **Quantitative real-time PCR** | |
| Q-IRP-F | TCACTACCTCCAGCACTCCG |
| Q-IRP-R | TGACCAATGGGCTCCTTCTC |
| Q-Fer-1F | GGGAATGGTGATGCTGATGTA |
| Q-Fer-1R | AAAGCTCCTTGTCAAAGATACC |
| Q-Fer-2F | GTCACGAAGAAAATACATGAAGTG |
| Q-Fer-2R | TGCTGATACCTTACAACTCCC |
| Q-actin-F | GCATCCACGAGACCACTTACA |
| Q-actin-R | CTCCTGCTTGCTGATCCACATC |
| **RNA interference** | |
| si*Es*IRP | CGCUGACCUUGUGAUUGAU |
| si*Es*Fer-1 | CGAGCAGUAACCAGAAACU |
| si*Es*Fer-2 | GCAGCAAGCCAUAUCAUAC |
| siGFP | UAAUACGACUCACUAUAGGG |

web.expasy.org/protparam/). Signal peptides and transmembrane helices were predicted using SignalP 4.1 (http://www.cbs.dtu.dk/services/SignalP/) and TMHMM 2.0 (http://www.cbs.dtu.dk/services/TMHMM/), respectively. The structure and function of domains were predicted using SMART (http://smart.embl-heidelberg.de/), and three-dimensional models were constructed using SWISS-MODEL (http://swissmodel.expasy.org/). Multiple sequence alignment was performed using the DNAMAN software. A phylogenetic tree was constructed based on the alignment of amino sequences using the neighbor-joining method with 1000 bootstrap replications in MEGA 7.0.

### 2.6. qRT-PCR

To determine the tissue distribution of *Es*IRP, we used qRT-PCR with specific primers Q-IRP-F and Q-IRP-R (Table 1). Q-actin-F and Q-actin-R (Table 1) were used to amplify β-actin as the internal control [25]. qRT-PCR was performed using the SYBR Premix Ex Taq™ Kit (Takara), according to manufacturer's instructions, in a CFX96 Real-Time system (Bio-Rad, Hercules, CA, USA). Relative expression levels were calculated and quantified using the comparative CT ($2^{-\Delta\Delta Ct}$) method. Statistical analysis was performed using SPSS. Data represent mean ± standard error. Statistical significance was determined using one-way analysis of variance (ANOVA) and post hoc Duncan multiple-range tests. Statistical significance was set at $P < 0.05$. For analyzing the expression of *Es*IRP, *Es*Fer-1, and *Es*Fer-2 after bacterial challenge, the reaction conditions were as described above. Data were analyzed using unpaired *t*-test, and statistical significance was set at $P < 0.05$.

### 2.7. RNAi assay

Based on the sequences of the *Es*IRP, *Es*Fer-1, and *Es*Fer-2 genes, small interfering RNAs (siRNAs) specifically targeting each gene were synthesized using an *in vitro* transcription T7 kit, according to manufacturer's instructions (Takara). The sequences of siRNAs were displayed in Table 1. GFP siRNA was used as the negative control. The synthesized siRNAs were dissolved in siRNA buffer (50 mM Tris–HCl, 100 mM NaCl, pH 7.5) and quantified using spectrophotometry. RNAi assay was performed by injecting 100 μg siRNA into the foot of the third appendage using a syringe. At 24 h after the injection, hemocytes were collected. The efficacy of the RNAi procedure was assessed using qRT-PCR. The assays were biologically repeated three times.

### 2.8. Bacterial clearance assay

Healthy crabs were randomly divided into three groups depending on whether they were injected with siRNAs of *Es*Fer-1, *Es*Fer-2, or GFP. Bacterial suspensions (*S. aureus* and *V. parahemolyticus*) were cultured overnight in LB broth at 37 °C and adjusted to OD 600 = 0.2. After washing with PBS, the bacteria were collected by centrifugation at 5000 × *g* for 5 min and resuspended in 200 μl of PBS, then injected into each crab in different groups, and the hemolymph was collected at 24 h post-injection. After serial dilution, the number of residual bacteria was determined by plating the samples onto LB agar plates. Three to five crabs were used in each group, and each experiment was repeated three times. The results are presented as the mean ± SD.

## 3. Results

### 3.1. cDNA cloning and sequence analysis of EsIRP

The length of the *Es*IRP cDNA sequence (GenBank accession: MK184455) cloned from *E. sinensis* hemocytes was 4474 bp, and it included a 2682-bp ORF along with 51 bp 5′-UTR and 1741 bp 3′-UTR. *Es*IRP cDNA and the deduced amino acid sequences are shown in Fig. 1A. The ORF was found to encode 893 amino acids. The predicted molecular weight of the *Es*IRP protein was 98.36 kDa and the estimated pI was 6.05. As identified via SignalP 4.1 and TMHMM 2.0, neither signal peptides nor transmembrane helices were observed. SMART predicted that the 59 to 570 and the 698 to 827 amino acid residues were aconitase and aconitase C-terminal domains, respectively (Fig. 1B).

Three-dimensional models of *Es*IRP were constructed using SWISS-MODEL. A hypothetical protein was subjected to a BLAST search against PDB database. PDB alignment showed that *Es*IRP (6–892 amino acids) shared the highest similarity (69.72%) with human IRP (PDB ID: 2b3y.1). Subsequently, the protein structure was homology modeled and showed by PyMol1.3. The structures of IRPs from different species indicated a very high similarity (Fig. 2).

### 3.2. Homologous and phylogenetic analysis of EsIRP

BLASTp analysis showed that *Es*IRP had the highest similarity (84%) with the IRP of *Pacifastacus leniusculus*, followed by 74% similarity with cytoplasmic aconitate hydratase of *Lingula anatine*. Multiple protein sequence alignment analysis of the *Es*IRP amino acid sequence with other species revealed that IRPs have conserved functional domains in different species (Fig. 3). A phylogenetic tree was constructed based on the deduced amino acid sequences of IRPs from 20 species using MEGA 7.0. Sequences from mammals, bony fishes, molluscs, and crustaceans comprised the first group, followed by insects and then bacteria. *Es*IRP sequence was included in the first group, along with the crustaceans (Fig. 4).

### 3.3. Tissue distribution of EsIRP mRNA

SYBR green real-time PCR analyses were employed to quantify *Es*IRP mRNA expression in the hepatopancreas, stomach, gill, muscle, intestine, heart, and hemocytes. The mRNA of *Es*IRP was widely expressed in all samples. The highest expression level of *Es*IRP was detected in the muscle, followed by the intestine. The lowest expression level of *Es*IRP was noted in the gill (Fig. 5).

### 3.4. Transcription level changes in EsIRP after bacterial challenge

To investigate the role of *Es*IRP in the immune response to *S. aureus* and *V. parahaemolyticus*, the transcription level of *Es*IRP mRNA from hemocytes was tested using qRT-PCR at different time periods after bacterial challenge; β-actin was used as the internal control. The relative expression levels of *Es*IRP were significantly downregulated after *S. aureus* (Fig. 6A) and *V. parahaemolyticus* (Fig. 6B) challenge from 6 h to 48 h; the PBS group served as the control.

### 3.5. EsFer-1 and EsFer-2 expression after bacterial challenge

For investigating the role of the IRP–IRE signaling pathway in the immune response to *S. aureus* and *V. parahaemolyticus*, the transcription level of *Es*Fer-1 and *Es*Fer-2 mRNA from hemocytes was tested using qRT-PCR at different time periods after bacterial challenge. In response to *S. aureus* and *V. parahaemolyticus* challenge, *Es*Fer-1 expression markedly increased from 6 h to 48 h ($P < 0.01$), being the highest at 12 h and 6 h, respectively (Fig. 7A). *Es*Fer-2 expression also showed a significant increase ($P < 0.01$) after *S. aureus* and *V. parahaemolyticus* challenge, and the expression was the highest at 6 h and 48 h, respectively (Fig. 7B).

### 3.6. EsIRP knockdown promoted EsFer-1 and EsFer-2 expression

To study the relationship between IRP and IRE, *Es*IRP expression was silenced using RNAi. *Es*IRP expression in the siRNA interference group was suppressed significantly in *E. sinensis* hemocytes at 24 h in comparison with the expression in the GFP RNAi group (Fig. 8A).

After *Es*IRP gene knockdown, *Es*Fer-1 and *Es*Fer-2 expression levels


**Fig. 1.** (A) Nucleotide and deduced amino acid sequences of *Es*IRP. The nucleotide sequence is numbered from the 5′-end, and the amino acid code is present below the corresponding codon. Aconitase domains are underlined. Aconitase_C domain is indicated by a wavy line. Start and stop codons are marked in bold. (B) Domain structure analysis of the putative *Es*IRP protein, which includes an aconitase domain in the N-terminus and an aconitase_C domain in the C-terminus.

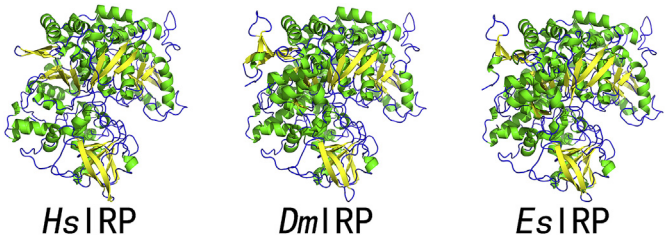


**Fig. 2.** A comparison of the three-dimensional structures of iron regulatory proteins from *Homo sapiens*, *Drosophila melanogaster*, and *Eriocheir sinensis*. The alpha-helix structure is highlighted in green, beta sheet in yellow, and L-loop in blue. (For interpretation of the references to colour in this figure legend, the reader is referred to the Web version of this article.)

were detected using qRT-PCR. In response to *Es*IRP knockdown, *Es*Fer-1 and *Es*Fer-2 expression significantly increased to levels higher than those observed in the GFP RNAi group (Fig. 8B and C). This indicated that *Es*IRP knockdown results in increased expression of *Es*Fer-1 and *Es*Fer-2 in *E. sinensis*.

### 3.7. *EsFer-1 and EsFer-2 knockdown inhibits bacterial clearance*

To investigate the *in vivo* function of the IRP–IRE signaling pathway in *E. sinensis*, RNAi of *Es*Fer-1 and *Es*Fer-2 and bacterial clearance assays were performed. qRT-PCR analysis indicated that 24 h after siRNA injection, the mRNA level of *Es*Fer-1 and *Es*Fer-2 in hemocytes decreased significantly compared with that in the normal (i.e., without any

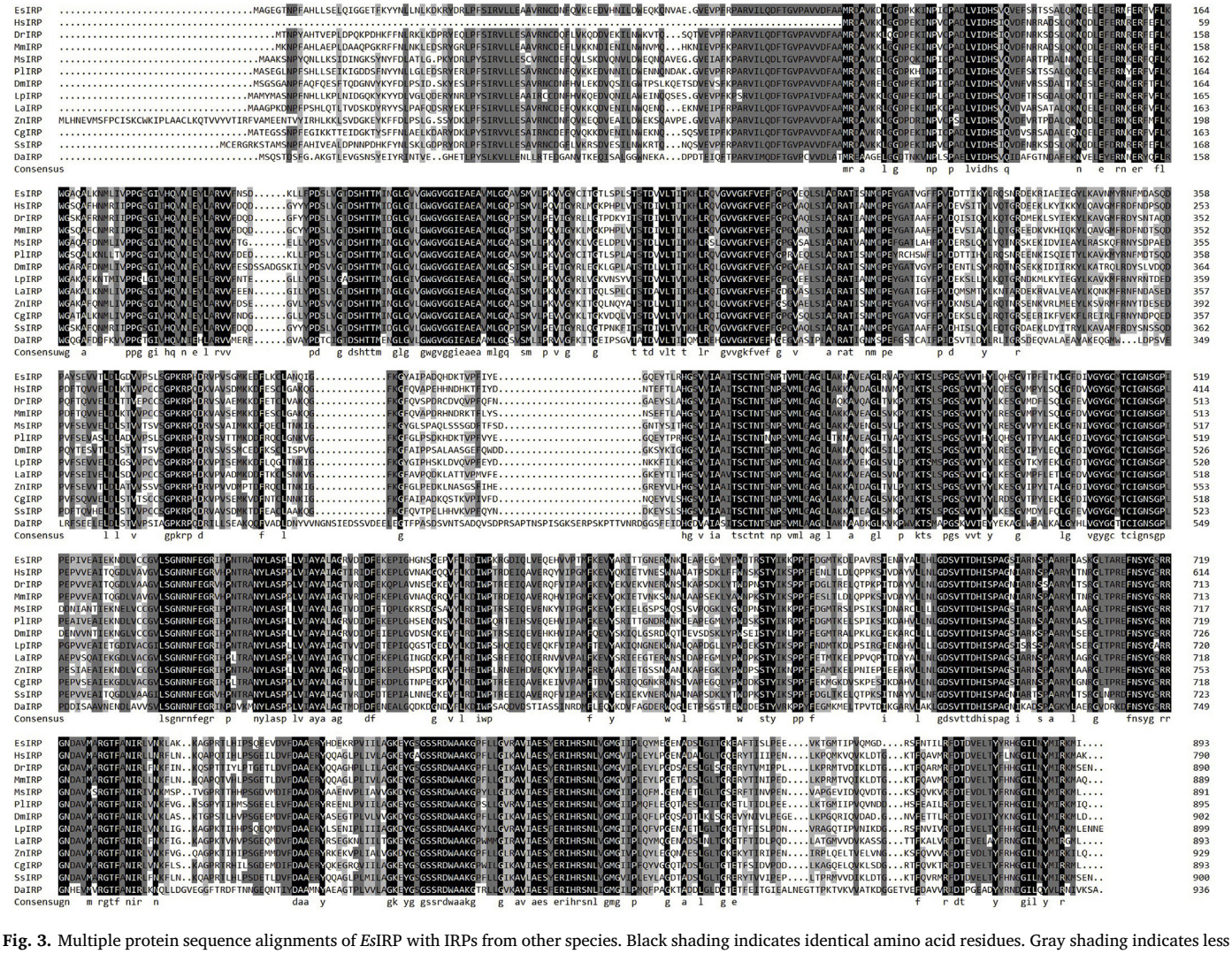

**Fig. 3.** Multiple protein sequence alignments of *Es*IRP with IRPs from other species. Black shading indicates identical amino acid residues. Gray shading indicates less conserved residues. Pale gray shading indicates somewhat similar residues. Sequences and their accession numbers are as follows: *HsIRP*, *Homo sapiens* AAF99681.1; *DrIRP*, *Danio rerio* AAZ30732.1; *MmIRP*, *Mus musculus* NP_031412.2; *MsIRP*, *Manduca sexta* AAK39637.1; *PlIRP*, *Pacifastacus leniusculus* CAB41634.1; *DmIRP*, *Drosophila melanogaster* CAA11211.1; *LpIRP*, *Limulus polyphemus* XP_013787464.1; *LaIRP*, *Lingula anatine* XP_013409790.1; *ZnIRP*, *Zootermopsis nevadensis* XP_021921229.1; *CfIRP*, *Crassostrea gigas* XP_011411873.1; *SsIRP*, *Salmo salar* ACI33729.1; and *DaIRP*, *Dermacoccus abyssi WP_118913250.1*.

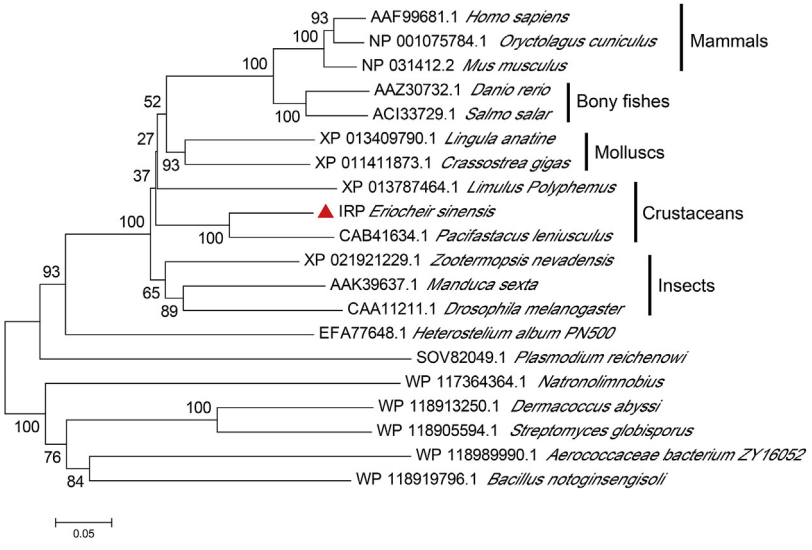


**Fig. 4.** Phylogenetic analysis of IRPs from various species. Scale bar corresponds to 0.5 estimated amino acid substitutions per site. *Es*IRP is highlighted using a red triangle. (For interpretation of the references to colour in this figure legend, the reader is referred to the Web version of this article.)

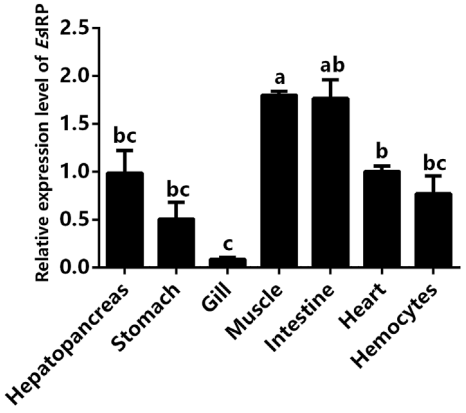


**Fig. 5.** Tissue distribution of *Es*IRP mRNA. Quantitative real-time RT-PCR results are shown; β-actin served as the reference gene. The different alphabets above each bar represent significant differences among bars and the same alphabets above different bars indicate no significant differences.

treatment) and GFP RNAi groups (Fig. 9A and B).

After *Es*Fer-1 and *Es*Fer-2 knockdown, *S. aureus* and *V. parahaemolyticus* were injected into *E. sinensis*. In response to this, the number of both *S. aureus* and *V. parahaemolyticus* CFU significantly increased in comparison with that in the GFP RNAi group (Fig. 9C and D). The bacterial clearance ability was thus impaired in *Es*Fer-1- and *Es*Fer-2-silenced crabs.

## 4. Discussion

Iron transport and storage are critical for host defense [26]. The binding of hepcidin to ferroportin inhibits iron export in a humoral manner [27]. IRPs regulate cellular iron metabolism; they interact with IREs of target mRNAs to regulate the translation of key iron metabolism genes encoding iron storage proteins and the iron exporter. Earlier studies have reported that the functions of IRPs are essential for organismal survival. For example, mice completely lacking IRP in their hepatocytes or duodenal enterocytes have been reported to die in the early postnatal period [28,29]. The function of the IRP–IRE system is important for macrophage-mediated immunity and host resistance to infection with intracellular bacteria [30]. Therefore, the IRP–IRE signaling pathway may play an important role in conferring innate immunity against bacteria in *E. sinensis*.

In this study, we successfully amplified the full-length cDNA of *Es*IRP using gene cloning and RACE techniques. *Es*IRP has aconitase domains, as predicted using SMART. IRP1 binds a [4Fe−4S] cluster and functions as cytosolic aconitase, which catalyzes the conversion of citrate to isocitrate in the cytosol [31,32]. Assembly and disassembly of the [4Fe−4S] cluster can regulate IRP1 activity by changing conformations. The aconitase family proteins have a four-domain organization. Domains 1, 2, and 3 of typical mitochondrial aconitases are tightly associated with each other to nestle the Fe−S cluster; in a subgroup of isopropylmalate isomerases, domain 4 is a separate, unlinked peptide chain. However, in the aconitase B group, the four domains are contiguous but cyclically permuted in the order 4-1-2-3 [33]. Three-dimensional models of IRPs indicated a very high similarity among *Es*IRP, *Dm*IRP, and *Hs*IRP. Multiple sequence alignment and phylogenetic tree analysis showed that *Es*IRP has a close genetic relationship with other species and it is highly conserved evolutionarily. In mammals, IRP stabilizes the transcripts of transferrin receptor by binding to IREs in the 3′-UTR. Transferrin receptor plays a critical role in cellular iron uptake [34,35]. In addition to vertebrates, IRPs have been identified in *Drosophila melanogaster* using electromobility shift assays [36]. Moreover, functional IREs have been identified in mRNAs encoding succinate dehydrogenase and ferritin in *D. melanogaster* [37]. These results suggest that the IRP − IRE signaling pathway operates in various species.

Our results showed that mRNA transcripts of *Es*IRP were widely distributed throughout the tested tissues in *E. sinensis*, which suggests that *Es*IRP plays an important role in maintaining iron homeostasis in various cells. The high expression of *Es*IRP in the intestine is probably due to the presence of beneficial microbial species. In humans, IRP expression is present in most tissues, such as the liver, lung, spleen, kidney, heart, duodenum, and brain [38]. It demonstrates that the IRP − IRE system can act as the major modulator of intracellular iron metabolism. Hepatopancreas plays a crucial role in immune defense against various pathogens in crustaceans. Therefore, it was used as the target tissue to examine the expression profiles of *Es*IRP after bacteria challenge. In *E. sinensis*, IREs were identified in the 5′-UTR of *Es*Fer-1 and *Es*Fer-2 mRNAs [23]. To investigate the role of the IRP–IRE signaling pathway in the immune response against bacteria, the transcription levels of *Es*IRP, *Es*Fer-1, and *Es*Fer-2 were analyzed in *E. sinensis* after *S. aureus* and *V. parahaemolyticus* challenge. Our results showed that the expression levels of *Es*IRP were downregulated whereas those of *Es*Fer-1 and *Es*Fer-2 were upregulated. IRPs can bind to IREs to control target mRNA translation. IREs have been found in the 5′- or 3′-UTR of mRNA transcripts of genes related to iron uptake, utilization, and storage [39]. IREs are RNA stem-loop structures composed of a conserved loop with the sequence CAGUGX (X = U, C, or A) [40]. The conformation of IRP changes when it binds IRE; IRP adopts an L-shape conformation to make a two-point contact with IRE. IRE binding sites use similar amino acids as the Fe−S cluster-binding region in aconitase [41]. This explains the mechanism of translation modulation by the IRP–IRE signaling pathway. The translation of transcripts is inhibited by the binding of IRPs to IREs in the 5′-UTR. When iron bind to IRPs, there are conformational changes that result in its dissociation from IREs. Subsequently, the translation of transcripts is promoted. If an IRE is present in the 3′-UTR, without IRP binding, transcripts can

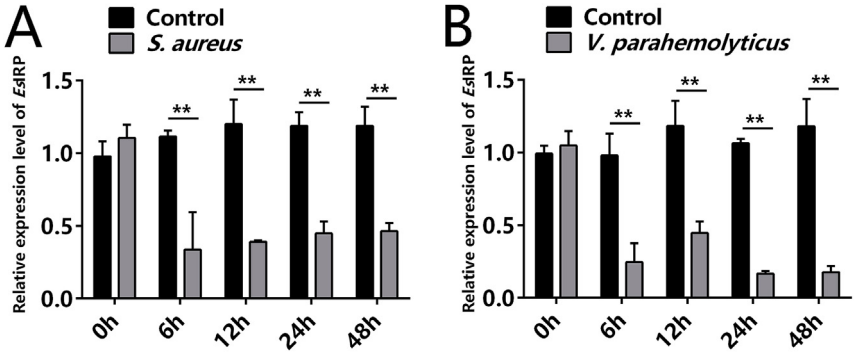


**Fig. 6.** Temporal expression of the *Es*IRP gene after *Staphylococcus aureus* (A) and *Vibrio parahaemolyticus* (B) challenge. Quantitative real-time RT-PCR results are shown. Statistically significant differences are indicated by asterisks (**$P < 0.01$).

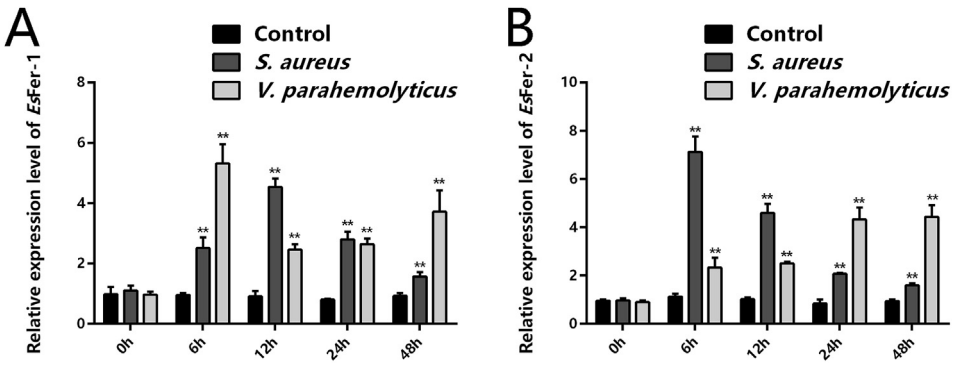


**Fig. 7.** Temporal expression of *Es*Fer-1 (A) and *Es*Fer-2 (B) after *Staphylococcus aureus* and *Vibrio parahaemolyticus* challenge. Quantitative real-time RT-PCR results are shown. Statistically significant differences are indicated with asterisks (**$P < 0.01$).

become susceptible to endonuclease attack and degradation; IRP binding to IRE in the 3′-UTR can thus protect transcripts from endonuclease degradation, promoting the translation of transcripts. When iron binds to IRPs, the dissociation of IRPs from IREs in the 3′-UTR downregulates the translation of transcripts. This mechanism corresponds to our observations in *E. sinensis*.

To investigate the function of the IRP–IRE signaling pathway in bacterial infections, we performed *Es*Fer-1 and *Es*Fer-2 RNAi and bacterial clearance assays. *Es*Fer-1 and *Es*Fer-2 knockdown attenuated the clearance of both *S. aureus* and *V. parahaemolyticus*. In infectious diseases, iron is essential both to the host and microbes: the host needs iron to modify immune effector mechanisms whereas microbes require it for proliferation [42,43]. Therefore, iron sequestration is an efficient mammalian defense strategy to inhibit the proliferation and pathogenicity of microbes. Iron overload on the other hand can increase the risk of bacterial infections. For example, in patients with thalassemia, blood transfusions reportedly contribute to iron overload, which increases the risk of infection with *Streptococcus pneumoniae*, *Pseudomonas aeruginosa*, *Klebsiella* species, *Yersinia* species, *Escherichia coli*, and *V. vulnificus* [44]. Hemolytic anemias including thalassemia also lead to tissue iron overload and an increase in serum iron levels. In a mouse model (*Hamp*$^{-/-}$ mice), iron overload was reported to lead to very rapid growth of *V. vulnificus*, eventually resulting in septicemia [45]. Many microbes possess receptors for hemoglobin, heme, ferritin, or transferrin to gain access to host iron sources. Haptoglobin and hemopexin can bind hemoglobin and heme for uptake, lowering iron availability for microbes. Transferrin is downregulated in case of an infection to lower the level of transferrin-bound iron. Serum ferritin may also be cleared by ferritin receptors. Therefore, macrophage and microbial ferritin receptors appear to directly compete for their iron-carrying ligand [46]. Many bacteria and certain fungi can produce siderophores, which are low molecular weight iron chelators with extremely high affinity for ferric iron. They are able to remove iron from host proteins, such as transferrin and ferritin, and are subsequently taken up by bacteria via specific receptors present across their outer membrane [47,48]. The expression of ferroportin-1 and ferritin reportedly increased and production of proinflammatory cytokines decreased upon infection with *Salmonella typhimurium* in IRP1- and IRP2-deficient myeloid cells [49].

In addition to iron ions, other metal ions are also involved in the innate immune response. In some bacteria, $Mn^{2+}$ can reduce oxidative damage to $Fe^{2+}$-containing proteins by replacing the more reactive $Fe^{2+}$ [50]. $Zn^{2+}$ is the second most abundant transition metal in most living systems and can serve both catalytic and structural roles within proteins [51]. Cu was accumulated at sites of infection in *Mycobacterium tuberculosis* pulmonary infections and resistance is necessary for *M. tuberculosis virulence* [52]. Therefore, defining the mechanisms and molecular machinery involved in the struggle for nutrient metals has the potential to uncover new therapeutic targets for the treatment of animal infections.

In summary, *Es*IRP was identified in *E. sinensis* and its mRNA transcripts were found to be widely distributed in various tissues. After bacterial challenge, the expression levels of *Es*IRP was downregulated whereas those of *Es*Fer-1 and *Es*Fer-2 were upregulated in hemocytes. After *Es*IRP knockdown, *Es*Fer-1 and *Es*Fer-2 expression increased. Moreover, *Es*Fer-1 and *Es*Fer-2 knockdown impaired the bacterial clearance ability of *E. sinensis*. Our results thus suggest that the IRP–IRE signaling pathway plays an important role in the innate immune system response in crabs.

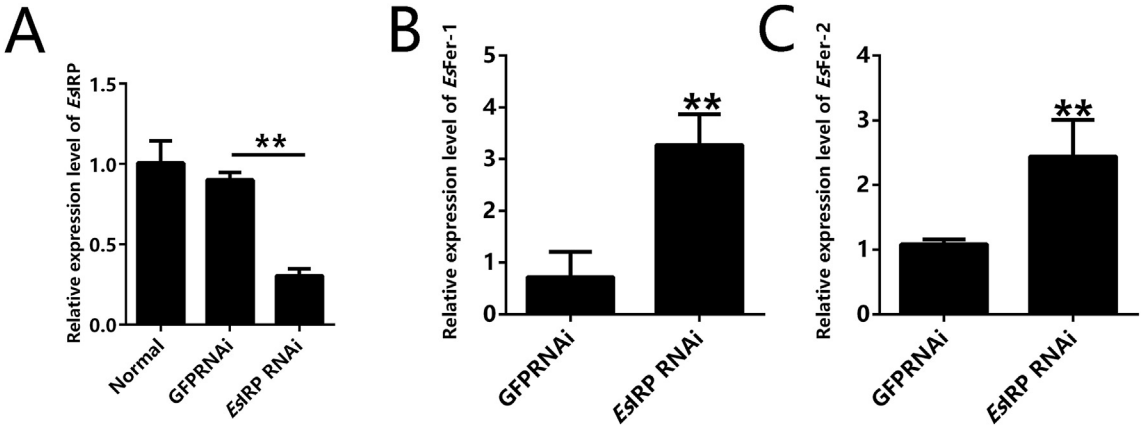


**Fig. 8.** *Es*Fer-1 and *Es*Fer-2 expression after *Es*IRP RNA interference (RNAi). (A) RNAi efficiency of *Es*IRP. (B) Transcription level of *Es*Fer-1. (C) Transcription level of *Es*Fer-2. GFP RNAi was used as the control. Statistically significant differences are indicated with asterisks (**$P < 0.01$).

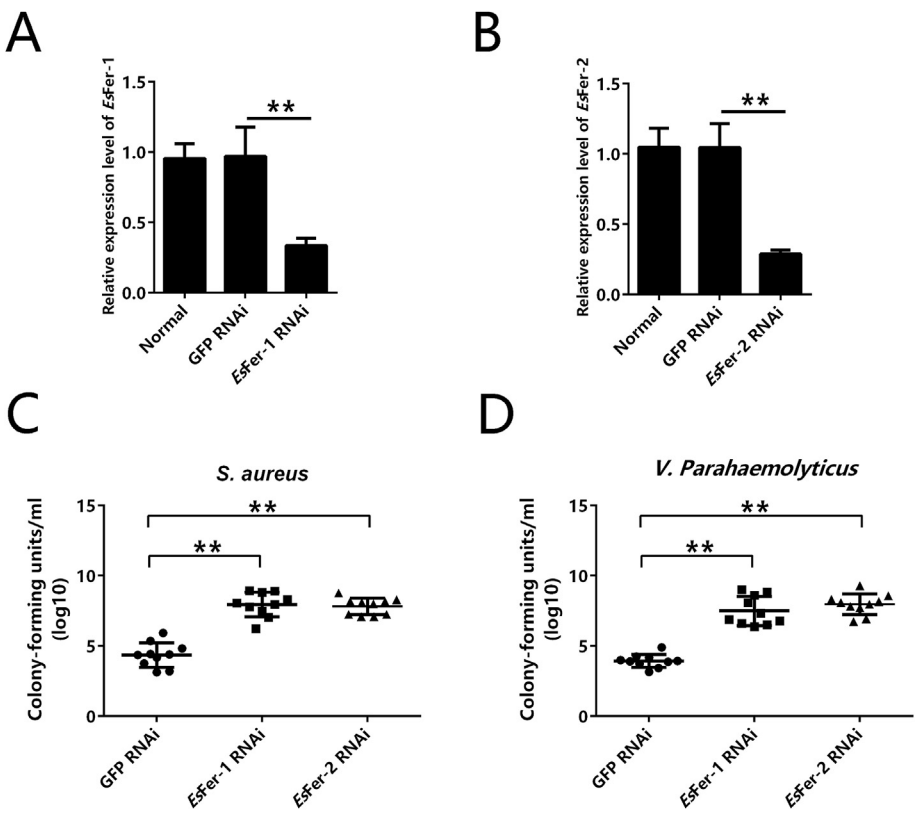


**Fig. 9.** Bacterial clearance ability of *Eriocheir sinensis* after *Es*Fer-1 and *Es*Fer-2 RNA interference (RNAi). RNAi efficiency of *Es*Fer-1 (A) and *Es*Fer-2 (B), as analyzed using qRT-PCR. Bacterial load was measured by counting colony-forming units at 24 h after *Staphylococcus aureus* (C) and *Vibrio parahaemolyticus* (D) challenge. GFP RNAi was used as the control. Statistically significant differences are indicated with asterisks (**$P < 0.01$).

## Acknowledgements

This study was supported by the National Natural Science Foundation of China (Grant No. 31602189 and 31672639).

## References

[1] R. Medzhitov, C.A. Janeway Jr., Innate immunity: impact on the adaptive immune response, Curr. Opin. Immunol. 9 (1) (1997) 4–9.
[2] S.T. Ong, J.Z. Ho, B. Ho, J.L. Ding, Iron-withholding strategy in innate immunity, Immunobiology 211 (4) (2006) 295–314.
[3] S.C. Andrews, A.K. Robinson, F. Rodriguez-Quinones, Bacterial iron homeostasis, FEMS Microbiol. Rev. 27 (2–3) (2003) 215–237.
[4] J.J. Bullen, The significance of iron in infection, Rev. Infect. Dis. 3 (6) (1981) 1127–1138.
[5] H. Oexle, E. Gnaiger, G. Weiss, Iron-dependent changes in cellular energy metabolism: influence on citric acid cycle and oxidative phosphorylation, Biochim. Biophys. Acta 1413 (3) (1999) 99–107.
[6] T. Ganz, Correction to: iron and infection, Int. J. Hematol. 107 (1) (2018) 122.
[7] M.U. Muckenthaler, S. Rivella, M.W. Hentze, B. Galy, A red carpet for iron metabolism, Cell 168 (3) (2017) 344–361.
[8] C. Volani, C. Doerrier, E. Demetz, D. Haschka, G. Paglia, A.A. Lavdas, E. Gnaiger, G. Weiss, Dietary iron loading negatively affects liver mitochondrial function, Metall : Integr. Biometal. Sci. 9 (11) (2017) 1634–1644.
[9] F.L. Brancatisano, G. Maisetta, M. Di Luca, S. Esin, D. Bottai, R. Bizzarri, M. Campa, G. Batoni, Inhibitory effect of the human liver-derived antimicrobial peptide hepcidin 20 on biofilms of polysaccharide intercellular adhesin (PIA)-positive and PIA-negative strains of Staphylococcus epidermidis, Biofouling 30 (4) (2014) 435–446.
[10] Z. Popovic, D.M. Templeton, Inhibition of an iron-responsive element/iron regulatory protein-1 complex by ATP binding and hydrolysis, FEBS J. 274 (12) (2007) 3108–3119.
[11] M.W. Hentze, M.U. Muckenthaler, B. Galy, C. Camaschella, Two to tango: regulation of Mammalian iron metabolism, Cell 142 (1) (2010) 24–38.
[12] K. Pantopoulos, Iron metabolism and the IRE/IRP regulatory system: an update, Ann. N. Y. Acad. Sci. 1012 (2004) 1–13.
[13] C.C. Philpott, M.S. Ryu, Special delivery: distributing iron in the cytosol of mammalian cells, Front. Pharmacol. 5 (2014) 173.
[14] M.P. Horowitz, J.T. Greenamyre, Mitochondrial iron metabolism and its role in neurodegeneration, J. Alzheimer's Dis. : JAD 20 (Suppl 2) (2010) S551–S568.
[15] T. Ganz, Cellular iron: ferroportin is the only way out, Cell Metabol. 1 (3) (2005) 155–157.
[16] B. Galy, D. Ferring-Appel, S. Kaden, H.J. Gröne, M.W. Hentze, Iron regulatory proteins are essential for intestinal function and control key iron absorption molecules in the duodenum, Cell Metabol. 7 (1) (2008) 79–85.
[17] G. Bruno, F.A. Dunja, S.W. Sauer, K. Sylvia, L. Sa?D, P. Herve, K.L. Stefan, G.N. Hermann-Josef, M.W. Hentze, Iron regulatory proteins secure mitochondrial iron sufficiency and function, Cell Metabol. 12 (2) (2010) 194–201.
[18] M. Nairz, D. Ferring-Appel, D. Casarrubea, T. Sonnweber, L. Viatte, A. Schroll, D. Haschka, F.C. Fang, M.W. Hentze, G. Weiss, Iron regulatory proteins mediate host resistance to Salmonella infection, Cell Host Microbe 18 (2) (2015) 254–261.
[19] L. Wang, L.E. Harrington, Selective modulation of TLR4-activated inflammatory responses by altered iron homeostasis in mice, J. Clin. Investig. 119 (11) (2009) 3322–3328.
[20] W. Wang, B. Wen, G.E. Gasparich, N. Zhu, L. Rong, J. Chen, Z. Xu, A spiroplasma associated with tremor disease in the Chinese mitten crab (Eriocheir sinensis), Microbiology 150 (Pt 9) (2004) 3035–3040.
[21] X. Li, Z. Jia, W. Wang, L. Wang, Z. Liu, B. Yang, Y. Jia, X. Song, Q. Yi, L. Qiu, L. Song, Glycogen synthase kinase-3 (GSK3) regulates TNF production and haemocyte phagocytosis in the immune response of Chinese mitten crab Eriocheir sinensis, Dev. Comp. Immunol. 73 (2017) 144–155.
[22] Z. Jia, M. Wang, X. Wang, L. Wang, L. Qiu, L. Song, Transcriptome sequencing reveals the involvement of reactive oxygen species in the hematopoiesis from Chinese mitten crab Eriocheir sinensis, Dev. Comp. Immunol. 82 (2018) 94–103.
[23] P. Kong, L. Wang, H. Zhang, Z. Zhou, L. Qiu, Y. Gai, L. Song, Two novel secreted ferritins involved in immune defense of Chinese mitten crab Eriocheir sinensis, Fish Shellfish Immunol. 28 (4) (2010) 604–612.
[24] X. Xu, Y. Liu, M. Tang, Y. Yan, W. Gu, W. Wang, Q. Meng, The function of Eriocheir sinensis transferrin and iron in Spiroplasma eriocheiris infection, Fish Shellfish Immunol. 79 (2018) 79–85.
[25] A.K. Dhar, R.M. Bowers, K.S. Licon, G. Veazey, B. Read, Validation of reference genes for quantitative measurement of immune gene expression in shrimp, Mol. Immunol. 46 (8) (2009) 1688–1695.
[26] M. Nairz, D. Haschka, E. Demetz, G. Weiss, Iron at the interface of immunity and infection, Front. Pharmacol. 5 (2014) 152.
[27] E. Nemeth, M.S. Tuttle, J. Powelson, M.B. Vaughn, A. Donovan, D.M. Ward, T. Ganz, J. Kaplan, Hepcidin regulates cellular iron efflux by binding to ferroportin and inducing its internalization, Science 306 (5704) (2004) 2090–2093.
[28] B. Galy, D. Ferring-Appel, S.W. Sauer, S. Kaden, S. Lyoumi, H. Puy, S. Kolker, H.J. Grone, M.W. Hentze, Iron regulatory proteins secure mitochondrial iron sufficiency and function, Cell Metabol. 12 (2) (2010) 194–201.
[29] B. Galy, D. Ferring-Appel, S. Kaden, H.J. Grone, M.W. Hentze, Iron regulatory proteins are essential for intestinal function and control key iron absorption molecules in the duodenum, Cell Metabol. 7 (1) (2008) 79–85.
[30] M. Nairz, D. Ferring-Appel, D. Casarrubea, T. Sonnweber, L. Viatte, A. Schroll, D. Haschka, F.C. Fang, M.W. Hentze, G. Weiss, B. Galy, Iron regulatory proteins mediate host resistance to Salmonella infection, Cell Host Microbe 18 (2) (2015) 254–261.
[31] M.C. Kennedy, L. Mende-Mueller, G.A. Blondin, H. Beinert, Purification and characterization of cytosolic aconitase from beef liver and its relationship to the iron-responsive element binding protein, Proc. Natl. Acad. Sci. U. S. A 89 (24) (1992)

11730–11734.
[32] D.J. Haile, T.A. Rouault, C.K. Tang, J. Chin, J.B. Harford, R.D. Klausner, Reciprocal control of RNA-binding and aconitase activity in the regulation of the iron-responsive element binding protein: role of the iron-sulfur cluster, Proc. Natl. Acad. Sci. U. S. A 89 (16) (1992) 7536–7540.
[33] J. Dupuy, A. Volbeda, P. Carpentier, C. Darnault, J.M. Moulis, J.C. Fontecilla-Camps, Crystal structure of human iron regulatory protein 1 as cytosolic aconitase, Structure 14 (1) (2006) 129–139.
[34] M. Muckenthaler, M.W. Hentze, Mechanisms for posttranscriptional regulation by iron-responsive elements and iron regulatory proteins, Prog. Mol. Subcell. Biol. 18 (1997) 93–115.
[35] M.W. Hentze, L.C. Kuhn, Molecular control of vertebrate iron metabolism: mRNA-based regulatory circuits operated by iron, nitric oxide, and oxidative stress, Proc. Natl. Acad. Sci. U. S. A 93 (16) (1996) 8175–8182.
[36] S. Rothenberger, E.W. Mullner, L.C. Kuhn, The mRNA-binding protein which controls ferritin and transferrin receptor expression is conserved during evolution, Nucleic Acids Res. 18 (5) (1990) 1175–1179.
[37] A. Charlesworth, T. Georgieva, I. Gospodov, J.H. Law, B.C. Dunkov, N. Ralcheva, C. Barillas-Mury, K. Ralchev, F.C. Kafatos, Isolation and properties of Drosophila melanogaster ferritin–molecular cloning of a cDNA that encodes one subunit, and localization of the gene on the third chromosome, Eur. J. Biochem. 247 (2) (1997) 470–475.
[38] M.L. Wallander, E.A. Leibold, R.S. Eisenstein, Molecular control of vertebrate iron homeostasis by iron regulatory proteins, Biochim. Biophys. Acta 1763 (7) (2006) 668–689.
[39] R. Leipuviene, E.C. Theil, The family of iron responsive RNA structures regulated by changes in cellular iron and oxygen, Cell. Mol. Life Sci. : CMLS 64 (22) (2007) 2945–2955.
[40] M. Sanchez, B. Galy, M.U. Muckenthaler, M.W. Hentze, Iron-regulatory proteins limit hypoxia-inducible factor-2alpha expression in iron deficiency, Nat. Struct. Mol. Biol. 14 (5) (2007) 420–426.
[41] W.E. Walden, A.I. Selezneva, J. Dupuy, A. Volbeda, J.C. Fontecilla-Camps, E.C. Theil, K. Volz, Structure of dual function iron regulatory protein 1 complexed with ferritin IRE-RNA, Science 314 (5807) (2006) 1903–1908.
[42] M.P. Soares, G. Weiss, The Iron age of host-microbe interactions, EMBO Rep. 16 (11) (2015) 1482–1500.
[43] H. Drakesmith, A.M. Prentice, Hepcidin and the iron-infection axis, Science 338 (6108) (2012) 768–772.
[44] C.T. Peng, C.H. Tsai, J.H. Wang, C.F. Chiu, K.C. Chow, Bacterial infection in patients with transfusion-dependent beta-thalassemia in central Taiwan, Acta Paediatr. Taiwanica = Taiwan er ke yi xue hui za zhi 41 (6) (2000) 318–321.
[45] J. Arezes, G. Jung, V. Gabayan, E. Valore, P. Ruchala, P.A. Gulig, T. Ganz, E. Nemeth, Y. Bulut, Hepcidin-induced hypoferremia is a critical host defense mechanism against the siderophilic bacterium Vibrio vulnificus, Cell Host Microbe 17 (1) (2015) 47–57.
[46] E.G. Meyron-Holtz, S. Moshe-Belizowski, L.A. Cohen, A possible role for secreted ferritin in tissue iron distribution, J. Neural Transm. 118 (3) (2011) 337–347.
[47] M. Seifert, M. Nairz, A. Schroll, M. Schrettl, H. Haas, G. Weiss, Effects of the Aspergillus fumigatus siderophore systems on the regulation of macrophage immune effector pathways and iron homeostasis, Immunobiology 213 (9) (2008) 767–778.
[48] S. Markus, B. Elaine, K. Claudia, S. Yasmin, L. Omar, E. Martin, W. Anja, H.N. Arst, H. Ken, H. Hubertus, Distinct roles for intra- and extracellular siderophores during Aspergillus fumigatus infection, PLoS Pathog. 3 (9) (2007) 1195–1207.
[49] M. Nairz, D. Ferring-Appel, D. Casarrubea, T. Sonnweber, L. Viatte, A. Schroll, D. Haschka, F. Fang, M. Hentze, G. Weiss, Iron regulatory proteins mediate host resistance to Salmonella infection, Cell Host Microbe 18 (2) (2015) 254–261.
[50] J.M. Sobota, J.A. Imlay, Iron enzyme ribulose-5-phosphate 3-epimerase in Escherichia coli is rapidly damaged by hydrogen peroxide but can be protected by manganese, Proc. Natl. Acad. Sci. U. S. A 108 (13) (2011) 5402–5407.
[51] H. Klaus, Bacterial zinc uptake and regulators, Curr. Opin. Microbiol. 8 (2) (2005) 196–202.
[52] W. Frank, A. David, T.B. Shrestha, H.D. Laurel, N. Scott, L. Gyanu, W. Ying, S.H. Bossmann, R.J. Basaraba, N. Michael, Copper resistance is essential for virulence of Mycobacterium tuberculosis, Proc. Natl. Acad. Sci. U. S. A. 108 (4) (2011) 1621–1626.